Organic & Biomolecular Chemistry

Cite this: *Org. Biomol. Chem.*, 2012, **10**, 6682

www.rsc.org/obc

PAPER

Time-dependent density functional theory (TDDFT) modelling of Pechmann dyes: from accurate absorption maximum prediction to virtual dye screening†

Eric Assen B. Kantchev,*[a] Tyler B. Norsten‡*[a] and Michael B. Sullivan[b]

Received 27th April 2012, Accepted 14th June 2012
DOI: 10.1039/c2ob25806d

The red Pechmann dye (λ_{max} = 550 nm) is the *exo*-dimer of 4-phenyl-3-butenolide connected at the α-carbon by a double bond in a *trans*-fashion. The ring system is easily rearranged to the *trans-endo*-fused bicyclic 6-membered lactone dimer (yellow). Both lactones can be singly or doubly amidated with primary amines leading to further colour changes. The nature of the core heterocycle (*exo- vs. endo*-; 5- or 6-membered ring), core heteroatom (O *vs.* N) and additional substituents on the phenyl ring allows for exquisite control over colour achievable within a single dye family. Herein we present a detailed investigation of the modelling of the electronic spectra of the Pechmann dye family by time-dependent density functional theory (TDDFT). Whereas pure Hartree–Fock (TDHF) *ab-initio* calculation underestimates the UV/Vis absorption maximum, pure TDDFT leads to a large overestimation. The accuracy of the prediction is highly dependent on the mix of HF and DFT, with BMK (42% HF) and M06-2X (54% HF) giving the closest match with the experimental value. Among all basis sets evaluated, the computationally-efficient, DFT-optimized DGDZVP showed the best chemical accuracy/size profile. Finally, the dispersion interaction-corrected (SMD) implicit solvation model was found to be advantageous compared to the original IEFPCM. The absorption maxima of substituted Pechmann dyes and their rearranged lactone counterparts can be predicted with excellent accuracy (±6 nm) at the optimal SMD(toluene)/TD-BMK/DGDZVP//SMD(toluene)B3LYP/DGDZVP level of theory. Using this procedure, a small virtual library of novel, heterocycle-substituted Pechmann dyes were screened. Such substitution was shown to be a viable strategy for colour tuning, giving λ_{max} from 522 (4-pyridyl) to 627 (2-indolyl) nm.

Introduction

Density functional theory (DFT) has emerged as a powerful computational methodology to evaluate and predict molecular properties at relatively modest computational cost.[1] The two Hohenberg–Kohn theorems[2] form the basis of DFT: (1) the electron density (a function only of the 3 spatial coordinates) alone determines the potential (a functional), hence the wavefunction and all electronic properties of a molecule; (2) the density is variational – the minimum energy is produced by only one, "correct" density functional. However, the exact form of this functional is unknown. Many approximate DFT functionals have been developed and implemented in modern quantum chemical/molecular modelling software packages. Perdew has organized different levels of DFT methods in the form of an allegorical "Jacob's ladder" from "Earth of Hartree" to "Heaven of chemical accuracy".[3] Functionals that occupy higher rungs of the ladder are more computationally demanding and, in general, yield calculated quantities that are closer to experimental or high-level *ab-initio* values. However, one of the drawbacks arising from the approximate nature of current DFT methods is that the selection of the best functional is largely problem-dependent.[4]

One important scientific problem is the evaluation of electronic excitation and structure and properties of excited states arising thereby. Wavelengths of electromagnetic radiation required for electronic excitation fall in the UV and visible regions of the spectrum; the energy difference between the ground and excited electronic states determines the wavelength of the absorbed light. The human eye perceives the sample containing the absorbing molecule as coloured in the

[a]*Institute of Materials Research and Engineering, 3 Research Link, Singapore 117602. E-mail: kantcheveab@imre.a-star.edu.sg; Fax: +65 6872 0785; Tel: +65 6874 1324*
[b]*Institute of High Performance Computing, 1 Fusionopolis Way #16–16, The Connexis, Singapore 138632*

†Electronic supplementary information (ESI) available: Cartesian coordinates, SCF energies and thermodynamic data for optimized structures **1–12**, **19**, **22**, **25** and **26** at SMD($CHCl_3$)/B3LYP/DGTZVP level of theory and **13–18**, **20**, **21**, **23**, **24**, **27–39** at SMD(toluene)/B3LYP/DGDZVP level of theory. See DOI: 10.1039/c2ob25806d

‡Current address: Linxens, 22 Changi North Way, Singapore 498810. tyler-brian.norsten@linxens.com; Fax: +65 6542 8835; Tel: +65 6579 1681.

complementary colour. Molecular structure is the primary determinant of electronic energy levels, thus it is possible to create structures (dyes) with tailored absorption maxima. Since the mid 19th century, an enormous range of dyes have been synthesized.[5] Recently, advances in molecular electronics, organic photovoltaic materials and bioimaging have led to renewed interest in organic dyes and theoretical studies thereof.[5a]

The extension of DFT to electronic excitation is the based on the Runge–Gross theorem,[6] which enables calculation of the electron density as a function of the three spatial coordinates and time, giving rise to the time-dependent DFT (TDDFT) method.[7] Electromagnetic radiation (light) is treated as an external potential that gyrates in a time-dependent manner with a single frequency. At present, TDDFT is the most useful method for calculation of the excited states and modelling of UV/Vis absorption spectra of a wide spectrum of large molecules.[8] Despite some well-known limitations of TDDFT for specific cases, generally excellent agreement with experiment or high level *ab initio* methods is attained. A number of recent studies of the electronic transitions of organic dyes[9] by TDDFT have appeared in the literature. Even though TDDFT can be used for *in-silico* evaluation of novel dyes even before their synthesis, such applications are still very rare and specialized.[10]

Pechmann dye (**1**) was serendipitously discovered by Hans von Pechmann in 1882.[11] The structure of **1** was a subject to controversy for another 42 years until it was conclusively determined to be a 4-phenyl-3-butenolide dimer joined by an *exo*-double bond at the α-carbon in a *trans*-fashion (Fig. 1).[12] Pechmann dye (**1**) can be thermally rearranged in protic solvents, or under basic conditions[13] to an *endo*-fused 6-membered dilactone (**2**) with a concomitant hypsochromic shift of the absorption maximum resulting in a colour change from red to orange–yellow. Both lactones are fluorescent (in yellow and green, respectively) in nonpolar solvents. Furthermore, stage-wise, twofold amidation of the Pechmann dye leads to a bathochromic shift in the corresponding lactams **3** and **4** (purple) but a hypsochromic shift in the rearranged analogs **5** and **6** (yellow).[14–16] Thus, judicious tuning of the core chromophore heterocycle (*exo-trans*-fused 5-membered rings, or *endo-trans*-fused 6-membered rings), aryl substituent and core rings heteroatoms (N *vs.* O) renders a wide range of colors possible with a single dye family. Despite the potential of Pechmann dyes, they never became commercial and after the 1950s[17] were almost forgotten. Moreover, no heteroaryl-substituted Pechmann dyes were ever explored until we published the first example very recently.[18] As a part of our efforts to discover novel Pechmann dye-related of compounds for optoelectronic applications,[18,19] we present herein a detailed characterization of Pechmann dyes by modern DFT calculations in ground and excited states followed by the use of the optimized TDDFT protocol for *in-silico* evaluation of hitherto unknown heteroaryl Pechmann dyes.

Results and discussion

2.1. Ground state structures of Pechmann dyes

The structure of the original, phenyl substituted Pechmann dye (**1**) was optimized at the *de facto* DFT standard[4] B3LYP functional using the computationally efficient, DFT-optimized, "double ζ + valence polarization" basis set equivalent to the one used in DGauss software ("DGDZVP").[20,21] In gas phase, the expected planar structure (dihedral angle C(6)–C(5)–C(7)–C(8) = 0.0°; 1.2° by X-ray crystallography[22]) comprising the completely conjugated phenyl-core chromophore-phenyl was observed. At this level of theory, the DFT-optimized structure matches very closely the single crystal X-ray structure. DFT bonds are slightly longer, with maximum deviation +0.030 nm, mean signed deviation +0.008 nm and mean unsigned deviation 0.014 nm. The largest unsigned deviation in DFT bond angles is 1.1° and the mean unsigned deviation is 0.5°.

The structures of Pechmann dyes **1–6** (Fig. 2) and the corresponding idealized core chromophore heterocycles **7–12** (Fig. 3) were further refined at B3LYP/DGTZVP[20] (the triple-ζ analogue of DGDZVP basis) in implicit solvent (chloroform) by SMD[23] formalism. SMD is a novel, extensively parameterized variant of the popular IEFPCM[24] implicit solvation model designed for accurate thermochemistry that uses an improved set of van der Waals radii and correction for weak (dispersion) solvent–solute interactions. Not unexpectedly, the stabilities of the 5-member ring core chromophore heterocycles (**9**, **10**) increase upon two successive amidations (−16.7 and −14.7 kcal mol^{-1}, respectively) starting from **7**. All three 5,5-*exo*-heterocycles (**7**, **9** and **10**) also gain considerable stabilization when they rearrange to the corresponding 6,6-fused (**8**, **11** and **12**) counterparts (−12.7, −18.9 and −25.4 kcal mol^{-1}, respectively). The two successive amidations in the 6,6-*endo*-fused array (**8** to **11**, **11** to **12**) are even more exothermic than the corresponding 5,5-*exo* array (−22.9 and −21.2 kcal mol^{-1}, respectively), contrary to what can be expected from simple ring strain release arguments. Not surprisingly, these individual reactions are by-and-large enthalpy driven. Conjugation of the core chromophores to the two phenyls results in a systematic shift of the Δ*G* for these 7

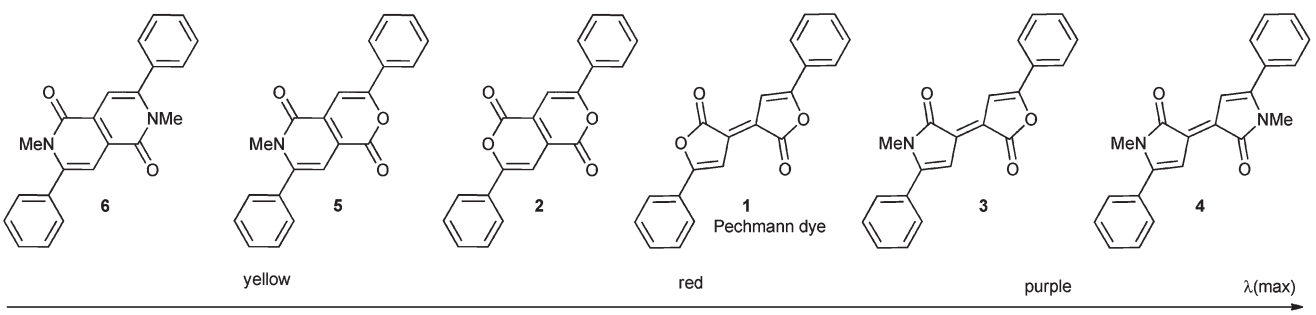

Fig. 1 Pechmann dye (**1**), ring-rearranged (**2**), *N*-methylamidated (**3**, **4**) and ring rearranged, *N*-methylamidated derivatives (**5**, **6**).

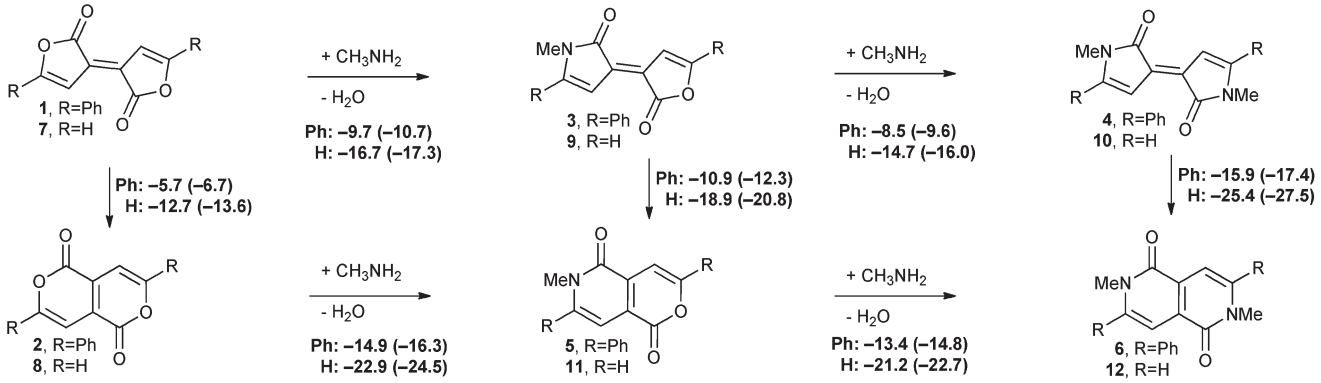

Fig. 2 Free energies (ΔG) and enthalpies (ΔH; in brackets) (kcal mol^{-1}) for the interconversion of various Pechmann dye compounds **1–6** (a) compared to the corresponding core chromophore heterocycles (**7–12**) (b) at SMD($CHCl_3$)/B3LYP/DGTZVP level of theory at 298 K.

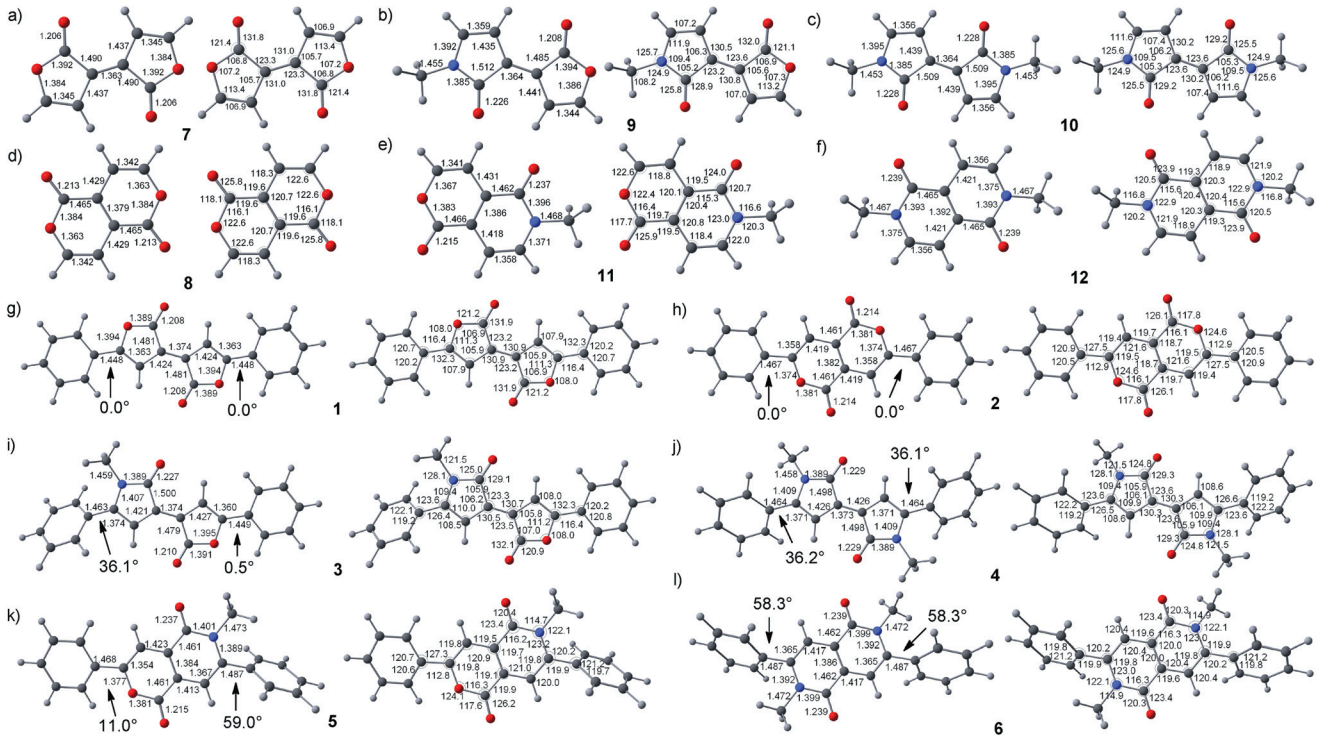

Fig. 3 Selected bond lengths (Å) and bond angles (°) of Pechmann dye core chromophores (**7–12**) and Pechmann dyes (**1–6**) at SMD($CHCl_3$)/B3LYP/DGTZVP level of theory. Dihedral angles for phenyl-core chromophore torsion in **1–6** are also shown.

reactions by ~+7 to +10 kcal mol^{-1}, while the trends remain completely preserved. Chemically, the computed free energies for the interconversions of the various Pechmann dye chromophores support the observation made long ago by synthetic chemists that the 5,5-*exo* dilactone **1** (the original Pechmann dye) behaves as a "doubly vinylogous anhydride" providing an entry point into the rest of the Pechmann dye family. Access to structures **5** and **6** as well as 6,6-*endo*-fused dilactone (**2**) must, however, pass through "open forms" as the direct rearrangements are extremely difficult. Whereas the structures of the lactones are flat (Fig. 3; phenyl-core dihedral angle of 0.0°), amidation causes some degree of twisting, which is more pronounced in the *endo*-6,6-fused skeleton; the phenyl-core dihedral angles are 36.1° and 58.3° for the symmetrical lactams **4** and **6**, respectively. The unsymmetrical lactone-lactams **3** and **5** have similar phenyl-core chromophore dihedral angles at the lactam ring (36.1° and 59.0°, respectively) but, interestingly, show some deviation from coplanarity at the lactone portion of the molecule, the dihedral angles being 0.53° and 11.0°. Identical dihedral angle values resulted from multiple optimization runs from slightly different starting geometries and at very tight cut-offs. For the *exo*-*5*,*5*-series, conjugation with the phenyl leads to lengthening of the central single C–C bond from 1.364 Å in **7**, **9** and **10** to 1.374 Å in **1**, **3** and **4**. For the *endo*-*6*,*6*-series, the central bond lengthened upon conjugation with phenyl for the lactones (**8** → **2**, 1.379 → 1.382 Å) but shortened for their lactam counterparts (**11** → **5**, 1.386 → 1.384 Å and **12** → **6**, 1.392 → 1.386 Å).

Table 1 Evaluation of TDDFT methods in the prediction of the UV-Vis absorption maximum (λ_{max}) of the Pechmann dye (**1**) with DGDZVP basis in implicit solvent (IEFPCM, toluene). The structure was optimized with B3LYP at the same level of theory. TDHF data is presented for comparison

Functional	% HF	Type[a]	λ_{max} (nm)	Ref.
Experiment	—	—	**550**, **511**	13
SVWN5	0	LSDA	638	2,25
BLYP	0	GGA	635	26,27
BP86	0	GGA	632	26,28
BPBE	0	GGA	630	26,29
BPW91	0	GGA	631	26,30
BTPSS	0	GGA	630	26,31
BKCIS	0	GGA	635	26,32
PW91LYP	0	GGA	636	27,30
mPWLYP	0	GGA	635	27,33
G96LYP	0	GGA	632	27,34
PBELYP	0	GGA	635	27,29
OLYP	0	GGA	625	27,32
TPSSLYP	0	GGA	622	27,31
TPSSTPSS	0	GGA	618	31
HCTH	0	GGA	626	35
B97D	0	GGA+D	630	36
BB95	0	mGGA	639	23,37
VSXC	0	mGGA	608	38
τHCTH	0	mGGA	630	39,40
M06-L	0	mGGA	596	40
TPSSh	10	hmGGA	594	31
O3LYP	12	hGGA	596	27,41
B3LYP	20	hGGA	584	27,42
B3P86	20	hGGA	582	28,42
B3PW91	20	hGGA	582	30,42
B98	22	hGGA	578	43
PBE0	25	hGGA	570	29,37
B1B95	25	hmGGA	570	37
M06	27	hmGGA	578	44
BMK	**42**	**hmGGA**	**544**	45
BHandHLYP	50	hGGA	525	46
M06-2X	**54**	**hmGGA**	**533**	44
M06-HF	100	hmGGA	495	44
CAM-B3LYP	11 → 65[b]	LR + hGGA	537	47
LC-ωPBE	0 → 100[b]	LR + hGGA	498	48
LC-M06-L	0 → 100[b]	LR + hmGGA	486	44,49
ωB97X	16 → 100[b]	LR + hGGA	519	50
ωB97XD	22 → 100[b]	LR + hGGA + D	535	51
HF	—	—	524	52

[a] Legend: LSDA = local spin density approximation, GGA = gradient-generalized approximation, m = meta, h = hybrid, LR = long range-corrected, D = empirical correction for dispersion interaction. [b] Short → long distance.

2.2. Optimization of TDDFT functional for chemically accurate prediction of the UV-Vis absorption maximum of the Pechmann dye 1

The lack of a systematic way to improve the performance of DFT methods is one of the greatest drawbacks of DFT.[4] We, therefore, undertook an evaluation of a number of common DFT functionals (Table 1) and basis sets (Table 2) in TDDFT (singlets only) calculations on the structure of the Pechmann dye (**1**) optimized at IEFPCM(toluene)/B3LYP/DGDZVP level of theory. Compound **1** exhibits a vibronically-split absorption maximum (λ_{max}) at 550 and 511 nm in toluene. DFT methods are commonly graded along the Perdew *et al.*'s "Jacob's ladder".[3] Pure DFT methods such as LSDA (local spin-density approximation, *i.e.*, SVWN5; first rung of the ladder) and a number of GGA (generalized gradient approximation; second rung of the ladder) all overestimated the λ_{max} in a tight range (638–618 nm; Table 1). Among these methods, TPSSTPSS was the best at 618 nm followed by HTCH (a standalone, empirically-fit functional) at 626 nm. The 3rd rung of the ladder is occupied by meta-GGA (mGGA) functionals that have not only the first derivative of the energy (the gradient) of GGA functionals, but also the second derivative (or its mathematical equivalent τ, the kinetic energy of the electrons) as well as other empirically-derived corrections (*e.g.*, for dispersion interaction) in some cases. The mGGA functionals showed greater variation, from 639 nm with BB95 to 596 with the recent M06-L. Various DFT exchange functionals can be mixed with the *ab initio* Hartree–Fock (HF) method[53] (also referred to as "exact exchange") to further improve the accuracy of the calculation. This approach has resulted in the *de-facto* DFT standard B3LYP functional containing 20% HF (used in 80%[4] of all DFT publications). Evaluation of a variety of hybrid GGA (hGGA) and hybrid + meta-GGA (hmGGA) methods revealed that the % of HF mixed with the exchange functional is the most important factor in attaining good accuracy of the predicted λ_{max} value relative to the experiment regardless of the choice of exchange and correlation functional. Among all functionals tested, BMK (42% HF) and M06-2X (54% HF) gave the closest match to the experiment (544 and 533 nm, respectively) and were retained for further evaluation. The hybrid approach has been refined to include a variation in the % of HF depending on the distance (long range-corrected functionals). Evaluation of popular DFT methods of this type revealed uneven and non-systematic performance. Considering their higher computational cost, these methods were not used further in this work. For comparison, TDHF prediction underestimated the λ_{max} (524 nm). Dispersion interaction, not unexpectedly, showed no effect on electronic excitation prediction for both pure and hybrid DFT methods. To probe the effect of the % of HF exchange in the DFT-HF mix, we performed a stepwise adjustment of the percentage of HF mixed with pure BLYP, PBEPBE, TPSSTPSS and M06-L functionals (Fig. 4). As expected, the increase of the percentage of exact exchange led to a non-linear decrease of λ_{max} from 635, 631, 618 and 596 nm, respectively, to 465 ± 1 nm. This end point corresponds to time-dependent HFLYP, HFPBE, HFTPSS and HFM06-L(cor) (the correlation functional used in M06-L) functionals. The value for the latter is different from M06-HF, as M06-L seems to be parameterized differently from M06, M06-2X and M06-HF beyond simple adjustment of the % of exact exchange. Similarly, the value for M06 (27% HF) was 578, but for HF (30%)-M06-L mix – 538, and for M06-2X (54% HF) and HF (50%)-M06-L mix, the values were 533 and 507 nm, respectively. Unlike the M06 family, there was a good correspondence of the values for the other 3 functionals in their default hybrid forms, and the customized variable HF-pure functional mix. The plot of eV *vs.* % HF (Fig. 4b) was close to linear up to about 70% HF, whereas the plot of λ_{max} (Fig. 4a) had the expected "1/x" line shape due to the reciprocal relationship between the two units. Examination of the TDDFT outputs revealed that up to 70% of HF, the S_0 transition was only between the HOMO and LUMO orbitals (see 2.5). Thereafter, contributions from the transition of HOMO − 1 to LUMO + 1 for BLYP, PBEPBE, TPSSTPSS and that plus the HOMO − 4 to LUMO transition for M06-L began to appear with

concomitant distortion in the curves. This implies that the maximum % of HF exchange in TDDFT should be kept below 70% for accurate results and meaningful comparisons for this class of compounds.

The choice of basis set has a great impact on the DFT accuracy.[54] Generally, the larger the basis set, the more accurate the results. However, there is the trade off with computing time required as DFT methods scale from N^3 for the pure functionals to close to N^4 for the advanced hybrid-*meta* GGA functionals for a given number of basis functions (N).[4] Therefore, for expedient TDDFT evaluations required in the context of *in silico* screening of a virtual library of dye candidates, the smallest basis set that gives results of good chemical accuracy is preferred. We evaluated a number of common basis sets with the two best functionals that emerged after functional evaluation, BMK and M06-2X at the identical geometry for Pechmann dye **1** (Table 2). The full electron, DFT-optimized "double-**z**eta (ζ) **p**lus **v**alence **p**olarization" basis from DGauss (DGDZVP) showed excellent agreement with the experiment. The triple-ζ counterpart (DGTZVP) employing 1.5 times as many basis functions improved the accuracy by mere 2 nm. The Ahlrich's basis sets from Turbomole – SVP (comparable to DGDZVP), TZV, TZVP (comparable to DGTZVP) – performed less satisfactorily at double-ζ level, but almost equally at triple-ζ. The HF-optimized Pople sets of double-ζ quality (3-21G and 6-31G) were not satisfactory (509 and 531 nm, respectively). The inclusion of valence shell polarization for heavy atoms (6-31G(d)) or both heavy atoms and hydrogens (6-31G(d,p) did not improve the situation a great deal. On the other hand, the inclusion of diffuse functions on heavy atoms (6-31+G) or heavy atoms and hydrogens (6-31++G) gave predicted absorptions only 6 nm lower than experiment, at par with DGDZVP (with BMK) while employing a slightly smaller number of basis functions. For M06-2X, 6-31+G and 6-31++G were slightly less accurate (529 *vs.* 533 nm). The triple-ζ Pople basis sets (6-311G) followed identical trends. The Pople sets converge to 549 nm with BMK and 537 nm with M06-2X. Finally, Dunning's correlation-consistent basis sets primarily used in post-HF methods (cc-pVXZ, X = D or T for double- or triple-ζ, respectively) performed considerably worse when their large size is taken into account.

Table 2 Evaluation of basis sets in the TDDFT prediction of the UV-Vis absorption maximum (λ_{max}) of the Pechmann dye (**1**) with DGDZVP basis in implicit solvent (IEFPCM, toluene) with BMK and M06-2X functionals. The structure was optimized at IEFPCM (toluene)/B3LYP/DGDZVP level of theory

Basis set	N^a	λ_{max} (nm), BMK	λ_{max} (nm), M06-2X	Ref.
Experiment	—	**550**, **511**		13
DGDZVP	**360**	**544**	**533**	20,21
DGTZVP	540	546	535	20,21
SVP	396	532	521	55
TZV	372	540	527	55
TZVP	528	544	533	55
3–21G	240	509	496	56
6-31G	240	531	517	57
6-31G(d)	384	532	519	57
6-31G(d,p)	420	532	519	57
6-31+G	**336**	**544**	**529**	57
6-31++G	348	544	529	57
6-31+G(d)	480	547	534	57
6-31++G(d,p)	528	547	534	57
6-31+G(2df,pd)	900	549	538	57
6-311G	348	533	520	58
6-311G(d)	468	548	537	58
6-311+G(d)	564	548	537	58
6-311++G(d,p)	612	549	537	58
cc-pVDZ	396	522	533	59
cc-pVTZ	888	545	534	59

[a] N = number of basis functions.

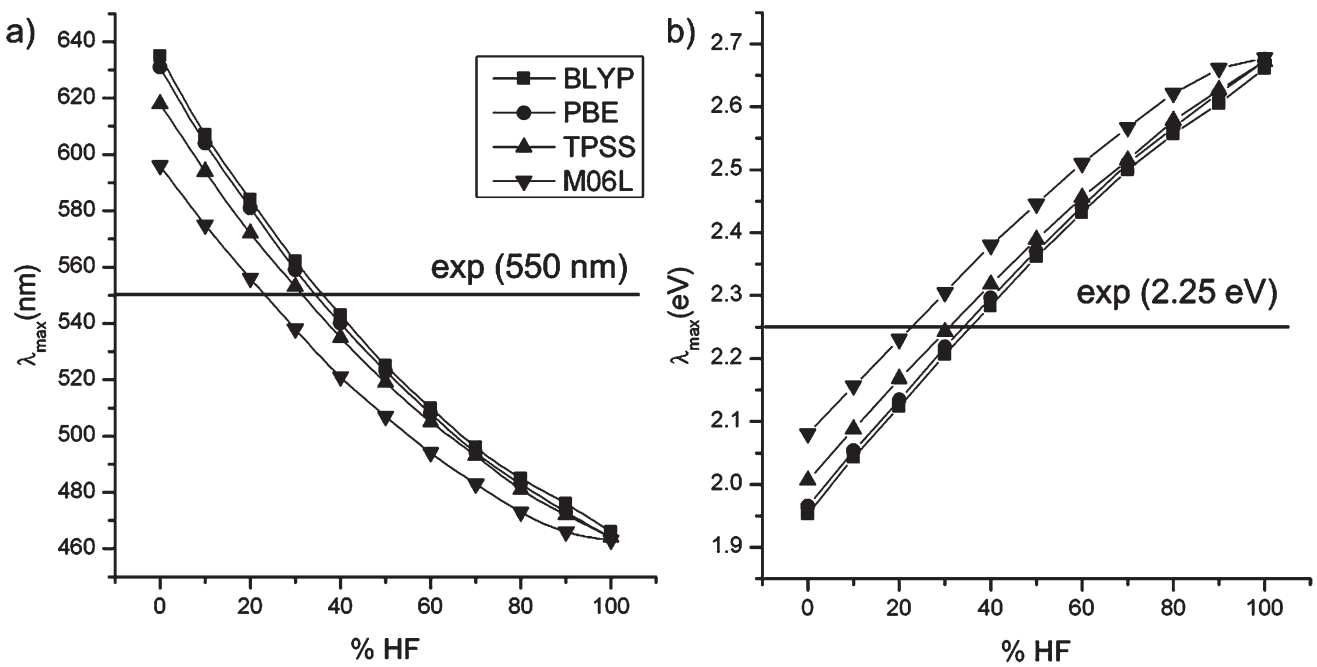

Fig. 4 Dependence of the absorption maximum of Pechmann dye (**1**) expressed in nm (a) and eV (b) on the % of Hartree–Fock exchange for 4 families of DFT functionals at IEFPCM(toluene)/TD((1 − *x*)DFT + *x*HF)/DGDZVP//IEFPCM(toluene)B3LYP/DGDZVP (*x* = 0 to 1, step = 0.1) level of theory.

Table 3 Evaluation of the best performing combinations of functional (M06-2X and BMK) and basis sets (DGDZVP, 6-31+G and 6-31+G(d)) for an extended set of Pechmann dyes (**1–6**, **13–18**; Fig. 2) in two implicit solvation models, IEFPCM and SMD. The performance at TD-M06/DGDZVP and TD-BMK/6-31+G(d) levels of theory is shown for comparison

		Solvation model		TD-DFT λ_{max} (nm) prediction at:					
Structure	Solvent	B3LYP opt.	TDDFT	M06/ DGDZVP	M06-2X/ DGDZVP	BMK/ DGDZVP	BMK/6-31+G	BMK/ 6-31+G(d)	λ_{max} (expt.) (nm)
1	Toluene	IEFPCM	IEFPCM	578	533	544	—	—	550, 511[13]
		IEFPCM	SMD	582	536	547	—	—	
		SMD	IEFPCM	579	534	544	—	—	
		SMD	SMD	583	536	548	547	550	
2	Toluene	IEFPCM	IEFPCM	463	427	433	—	—	434[13]
		IEFPCM	SMD	466	429	435	—	—	
		SMD	IEFPCM	463	426	432	—	—	
		SMD	SMD	466	429	434	429	435	
13	Toluene	IEFPCM	IEFPCM	613	561	575	—	—	588, 544[13]
		SMD	SMD	617	564	578	584	582	
14	Toluene	IEFPCM	IEFPCM	564	518	529	—	—	538, 507[13]
		SMD	SMD	567	521	532	527	533	
15	Toluene	IEFPCM	IEFPCM	492	447	456	—	—	454[13]
		SMD	SMD	494	449	458	455	459	
16	Toluene	IEFPCM	IEFPCM	455	417	424	—	—	478[13]
		SMD	SMD	458	421	427	418	427	
3	$CHCl_3$	IEFPCM	IEFPCM	599	561	570	—	—	550[16]
		SMD	SMD	608	569	578	578	582	
4	$CHCl_3$	IEFPCM	IEFPCM	601	564	573	—	—	562[16]
		SMD	SMD	611	574	582	578	587	
5	$CHCl_3$	IEFPCM	IEFPCM	423	391	395	—	—	425[16]
		SMD	SMD	425	393	396	390	397	
6	$CHCl_3$	IEFPCM	IEFPCM	386	359	360	—	—	394[16]
		SMD	SMD	389	361	363	354	362	
17	$CHCl_3$	IEFPCM	IEFPCM	626	589	597	—	—	632, 587[14]
		SMD	SMD	634	595	604	597	608	
18	$CHCl_3$	IEFPCM	IEFPCM	434	398	402	—	—	438, 412[14]
		SMD	SMD	438	401	405	394	402	

2.3. TDDFT studies of Pechmann dyes family of compounds

A more extensive set of Pechmann dyes and derivatives (**1–6**, **13–18**) was used to probe the robustness of the optimized TDDFT absorption maximum prediction. In addition, we compared the standard IEFPCM model with the recent SMD method that includes a correction for dispersion interaction (a traditional weakness of DFT) and an improved set of van der Waals atomic radii. For **1**, there was an improvement of the accuracy of λ_{max} prediction by 4 nm to 548 (experiment: 550 nm)[13] when SMD was used for both geometry optimization and TDDFT (Table 3). This effect was more pronounced for the TDDFT than for the structure optimization as demonstrated by mixed IEFPCM/SMD calculations for optimization/TDDFT, respectively, and *vice versa*. For the rearranged dilactone **2**,[13] using SMD in both computational steps increased the accuracy of the prediction from 433 to 434 nm (experimental value 434 nm). Similarly, for the *p*-methoxy analogs of **1** and **2**, (**7** and **9**) the accuracy was improved by 3 and 2 nm, respectively. For the *m*-nitro Pechmann dye **8**, the predicted and experimental values were also close, 532 *vs.* 538 nm. Interestingly, the *m*-nitro rearranged Pechmann dye **16** is reported to have λ(max) at 478 nm.[13] This violates two trends: first, the lactone rearrangement leads to ~115 nm hypsochromic shift and, second, inclusion of electron-donating substituents leads to a bathochromic shift, and of electron-withdrawing to a hypsochromic shift for both lactone series. In contrast, the TDDFT predicted value for **16** is 424 nm, very closed to the value of 423 nm predicted based on the absorption value for **9** (538–115 nm). The reasons for this discrepancy are unclear. The prediction accuracy diminished for the amidated analogs (**3–6**, **17** and **18**). For these compounds, BMK predictions were higher than the experimental values by 28 ± 7 nm, M06-2X – by 28 ± 13 nm and M06 – by 18 ± 29 nm. Generally, DGDZVP basis set was more accurate than 6-31+G and at par with the larger 6-31+G(d).

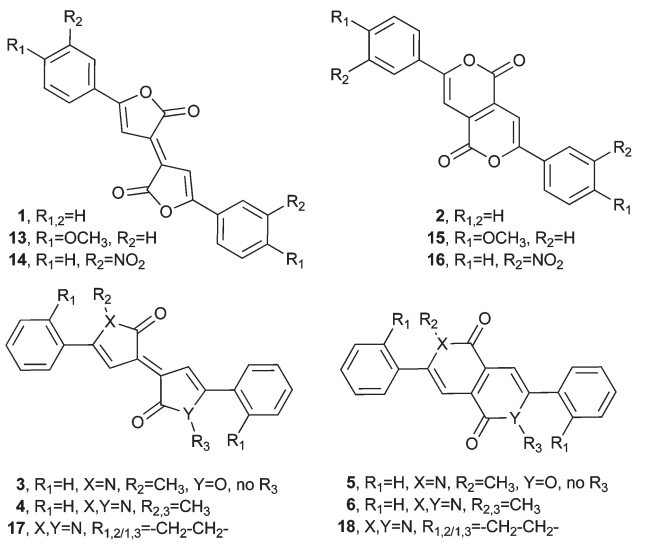

Recently, a synthetic route allowing preparation of one of the two "missing" heterocylic core isomers of **1** based on a

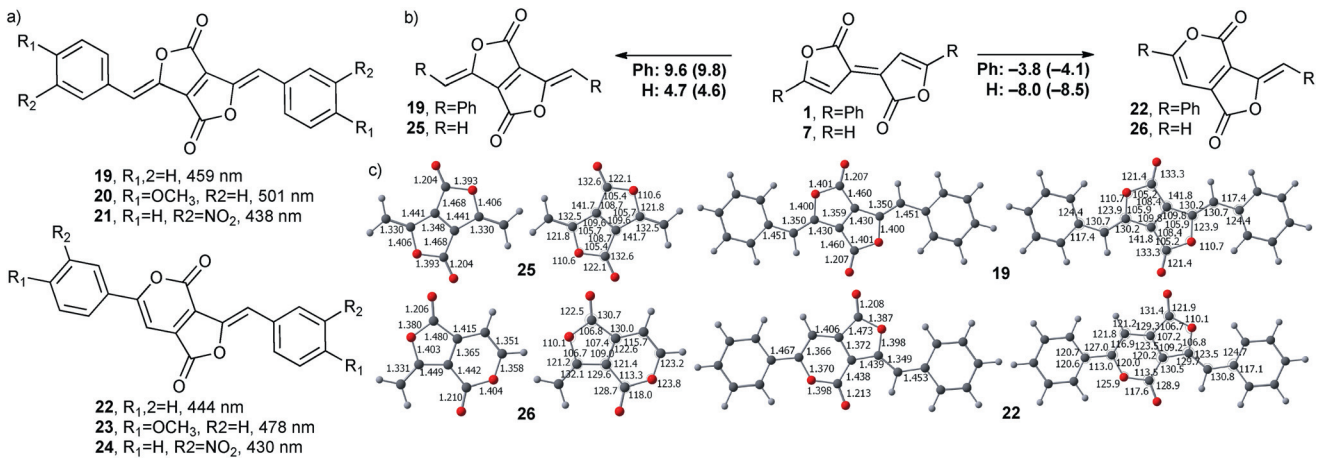

Fig. 5 (a) Predicted λ_{max} for the "unknown isomers" of the Pechmann dye, SMD(toluene)/TDBMK/DGDZVP//SMD(toluene)/B3LYP/DGDZVP level of theory. (b) Free energies (ΔG) and enthalpies (ΔH; in brackets) (kcal mol^{-1}, 298 K) relative to the parent Pechmann dye structures **1** and **7** and (c) structural plots and selected bond lengths (Å) and angles (°) at SMD($CHCl_3$)/B3LYP/DGTZVP level of theory.

transesterification–lactonization reaction of dimethyl 1,2-di(2-arylethinyl)fumarate was disclosed.[60] Therefore, we extended our study to include TDDFT evaluation of the hitherto unknown phenyl Pechmann dye isomers (**19** and **22**) and their *p*-methoxy- (**20** and **23**) and *m*-nitro-(**21** and **24**) substituted analogues (Fig. 5a) using our optimized TD-DFT procedure (SMD (toluene)/TDBMK/DGDZVP//SMD(toluene)/B3LYP/DGDZVP). A comparison of the TDDFT results for the dilactone representatives of the family revealed that the *p*-methoxy-substituted members underwent a bathochromic shifts (34 ± 4 nm) with respect to the unsubstituted (parent) members, whereas the *m*-nitro-substituted members – hypshochromic shifts (¬14 ± 7 nm). This is consistent with these lactones being relatively electron-poor as also demonstrated by their frontier orbital energies (see 2.5). Thermodynamically, the *endo*-5,5-lactones were less stable than the *exo*-5,5-lactones both at core chromophore (**7** → **25**) and phenyl conjugated forms (**1** → **19**), whereas the *endo*-5,6-lactones (**22** and **26**) were more stable than **1** and **7**, respectively (Fig. 5b). Interestingly, the *endo*-5,5-lactones were the only exception to the general rule that phenyl conjugation led to narrowing of the energy differences. Similar to the other Pechmann dyes, phenyl conjugation led to lengthening of the central C–C double bond in the *endo*-5,5- and *endo*-5,6-cores, from 1.348 Å to 1.359 Å and 1.365 Å to 1.372 Å, respectively. The *endo*-5,5-fused lactone series (**19**–**21**) was most sensitive to substitution, whereas the *endo*-6,6-fused system (**2**, **15** and **16**), the least. With respect to λ_{max} range, the ordering is *exo*-5,5-fused series (**1**, **13** and **14**) > *endo*-5,5 > *endo*-5,6 (**22**–**24**) > *endo*-6,6. The difference between *exo*-5,5 and *endo*-5,5 series was 77, 88 and 94 nm, between *exo*-5,5 and *endo*-5,6 was 100, 103 and 102 nm and *exo*-5,5 and *endo*-6,6 was 120, 114 and 105 nm for the *p*-methoxy, unsubstituted and *m*-nitro representatives. In addition, Nishihara *et al.* measured λ_{max} differences of *p*-(*N*,*N*-di-(*p*-methoxyphenyl)amino)phenyl-substituted series of 100 nm for *exo*-5,5 *vs.* *endo*-5,5 dilactones and 136 nm for *exo*-5,5 *vs.* *endo*-6,6 dilactones.[60] Similarly, we observed 112 nm difference between the 2-(3-dodecylthienyl)-substituted *exo*-5,5 and *endo*-6,6 dilactones.[19] These observations point that the contributions of substitution and core heterocycle type to λ_{max} are roughly constant and additive. Therefore, in the course of *in silico* design of new Pechmann dyes, evaluation of the original *exo*-5,5-dilactone (**1**)

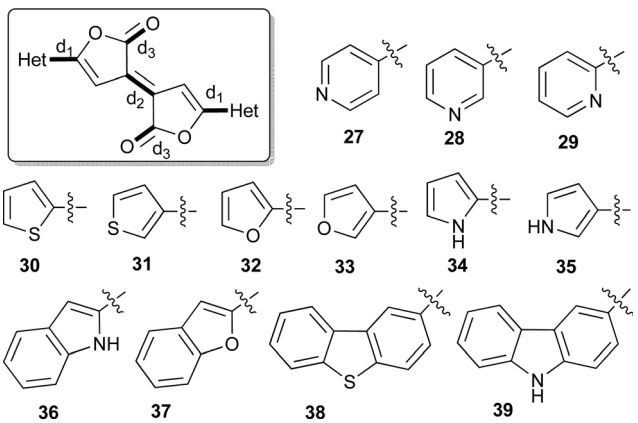

Fig. 6 Novel heteroaryl-substituted Pechmann dyes.

Table 4 TDDFT λ_{max} prediction for heteroaryl-substituted Pechmann dyes (**27**–**39**) at SMD($CHCl_3$)/TD-BMK/DGDZVP//SMD($CHCl_3$)/B3LYP/DGDZVP level of theory

Structure[a]	d_1 (Å)	d_2 (Å)	d_3 (Å)	λ_{max} (nm)[b]
1	1.453	1.379	1.211	547
27	1.455	1.377	1.209	522
28	1.453	1.378	1.210	535
29	1.458	1.378	1.209	532
30	1.432	1.381	1.211	576 (569)[c]
31	1.446	1.380	1.211	549
32	1.427	1.382	1.210	573
33	1.441	1.380	1.211	535
34	1.427	1.382	1.213	597
35	1.437	1.382	1.213	564
36	1.429	1.383	1.212	627
37	1.427	1.382	1.210	607
38	1.451	1.381	1.211	582
39	1.448	1.383	1.213	610

[a] Optimized at SMD(toluene)/B3LYP/DGDZVP level of theory. [b] At SMD(toluene)/TDBMK/DGDZVP level of theory. [c] Experimental value in brackets.

should, in principle, allow λ_{max} for the other core chromophore variations to be easily estimated.

2.4. *In silico* design of novel heterocyclic Pechmann dyes

Attaching a heteroaryl group with variable electronic properties to the Pechmann dye core chromophores enables tuning of the colour properties in a way that is synergistic and complementary with the substituent effects discussed above. In view of the scarcity of such compounds, we performed *in silico* screening of novel heteroaryl-substituted Pechmann dyes (Fig. 6). The λ_{max} prediction was carried out using our optimized TDDFT procedure. Besides the λ_{max} (predicted), the bond lengths of three key bonds (d_{1-3}) are presented (Table 4). The predicted λ_{max} for the pyridine-substituted Pechmann dyes was lower than the phenyl-substituted one (**1**) as expected for this electron-poor heterocycle. The hypsochromic shift diminished in the order 4 → 2 → 3-pyridyl. On the other hand, attachment of electron-rich 5-member heteroaryl substituents led to a pronounced bathochromic shift. The shift increased in the order pyrrole > thiophene > furan and 2 → 3-substituted. Extension of the conjugation by fusing an addition phenyl ring increased the predicted λ_{max} for 2-indolyl substituted Pechmann dye (**36**) to 627 nm, in the far red. 2-Benzofuryl (**37**) and 4-carbazolyl-substitued (**39**) analogues also showed substantial bathochromic shifts to 607 and 610 nm, respectively. For the only member of the virtual library synthesized to date (**30**), an excellent agreement between predicted (576) and recorded (569) λ_{max} value was observed. With respect to the structures, the d_1 bond showed the largest variation, being longer for pyridine-substituted Pechmann dyes (**27–29**: 1.453–1.458 Å) than for **1** (1.453 Å) but shorter for the other members of the virtual library (1.427–1.451 Å). The trends for the d_2 bond were in the opposite direction and lower in magnitude: shorter for pyridine-substituted dyes (1.377–1.378 Å) than for **1** (1.379 Å) but longer for the other members of the virtual library (1.380–1.383 Å). The carbonyl bond (d_3) was almost unchanged at 1.211 ± 2 Å. These structural variations can be qualitatively explained by charge-transfer from the heterocyclic substituent to the core chromophore.

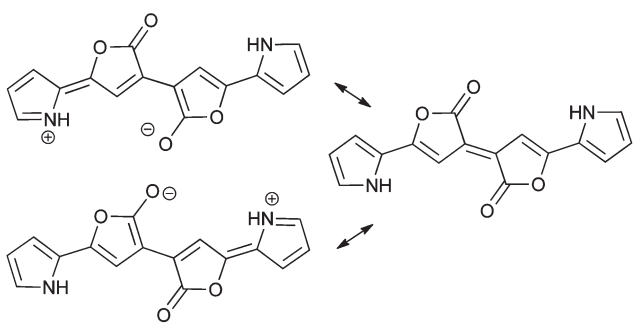

2.5. Frontier orbitals and excited states of Pechmann dye family of compounds

For the four isomeric dilactones (**1**, **2**, **19** and **22**), Kohn–Sham orbital 82 is the highest-occupied-molecular-orbital (HOMO) and 83 the lowest-unoccupied-molecular-orbital (LUMO) (Fig. 7). The HOMO and LUMO for **3** and **5** are 86 and 87 and for **4** and **6** are 90 and 91, respectively. Based on their symmetry, the frontier orbitals can be designated as π and π*, respectively. The amidation of the lactones leads to a repulsive steric interaction between the N-substituent and the *o*-hydrogen atoms of the phenyl ring (Fig. 3), which changes the degree of overlap between the core chromophore and the benzene ring. This can be observed by the diminishing orbital coefficients on the carbons of the benzene ring. The Kohn–Sham orbital eigenvalues (SMD($CHCl_3$)/BMK/DGDZVP//SMD($CHCl_3$)/B3LYP/DGDZVP level of theory) for compounds **1**, **3** and **4** (*exo*-5,5 series) suggest a very weak hypsochromic shift of the absorption maximum whereas a moderate bathochromic shift is observed experimentally. In contrast, for **2**, **5** and **6** (*endo*-6,6 series) there is a pronounced widening of the HOMO–LUMO gap due to the much stronger increases of LUMO energies than

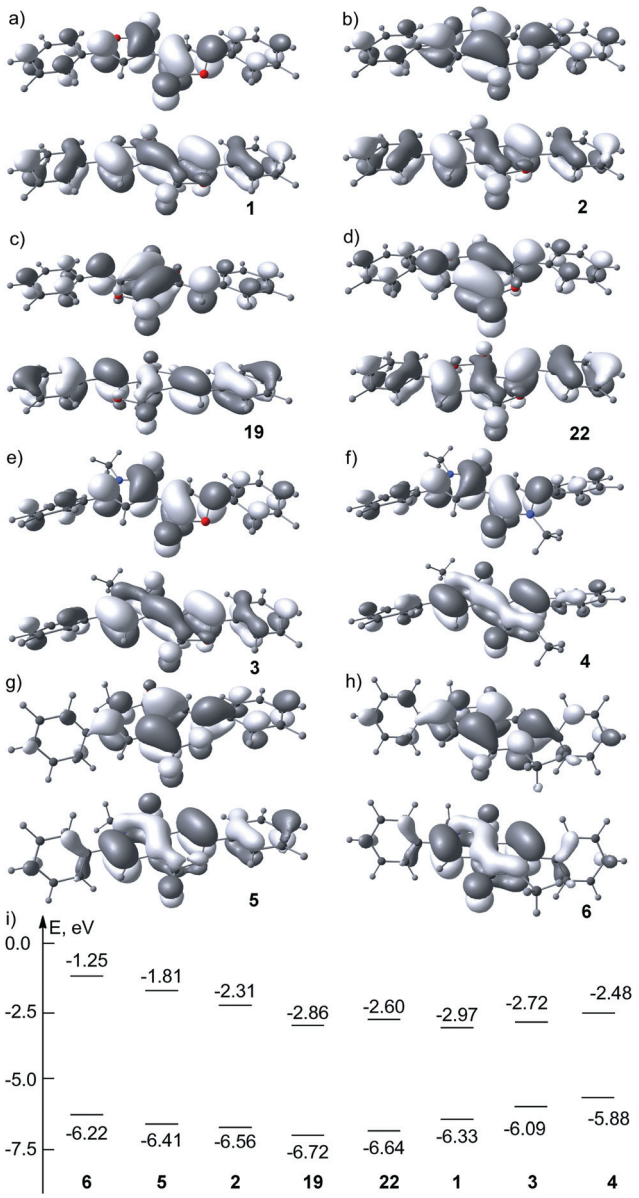

Fig. 7 Contour plots of HOMO (bottom), LUMO (top) for Pechmann dye compounds **1–6**, **13** and **16** (a–h) at SMD($CHCl_3$)/TD-BMK/DGDZVP//SMD($CHCl_3$)/B3LYP/DGDZVP level of theory. The frontier orbital energies are also shown (i).

HOMO, correctly identifying the relatively large hypsochromic shift observed experimentally. For structures **19** and **22**, the HOMO–LUMO bandgaps are between those for **1** and **2**, also as observed experimentally. The original Pechmann dye lactone (**1**) is the most electron-deficient representative of the series.

For compounds **1**, **2**, **19**, **22**, **4** and **6**, the π → π* (whole molecule) HOMO → LUMO (Table 5) transition was the most intense among the first 10 transitions as judged by highest oscillator strengths (f). The transition dipole moment (TDM) for this transition was large for all compounds implying significant charge redistribution during the excitation. For compound **1**, a second major transition was observed at 269 nm accompanied by a much weaker one at 271 nm, both being also of the π → π* (whole molecule) type. Two weak transitions at 308 nm of π → π* (phenyl → whole molecule) type and at 281 nm of π → π* (core chromophore only) were also found. For the rearranged lactone **2**, two strong π → π* (whole molecule) transitions at 301 and 242 nm and two weak, complex transitions at 275 and 232 nm of were additionally found. For compound **19**, a second major transition was observed at 245 nm accompanied by a somewhat weaker one at 243 nm, both being also of π → π* (whole molecule) and the second one also including π → π* (core chromophore → whole molecule) type. Also, one weak transition at 308 nm of π → π* (phenyl → whole molecule) type was found. Compound **22** showed the most complex electronic absorption of the set. There were three relatively weak transitions at 279, 258 and 249 nm of π → π* involving numerous whole molecule, core chromophore, phenyl and phenyl + core chromophore orbitals. These were complemented by two more transitions at 296 and 285 nm mostly of π → π* (phenyl → whole molecule) type. Lastly, a weak transition between HOMO − 1 and LUMO at 324 nm was also found. This is consistent with the planar, completely conjugated structures of **1**, **2**, **19** and **22**. For the lactam-type compound **4**, three transitions at 306 (very weak), 290 (strong), and 269 nm (moderately strong) all of π → π* (core chromophore → whole molecule) type as well as a single, weak π → π* (phenyl → whole molecule) at 284 nm transition were found. Surprisingly, for the twisted compound **6** having the largest phenyl-core chromophore dihedral angle, all secondary transitions (one fairly strong at 286 nm and 3 weak at 244, 238 and 230 nm) were of the π → π* (whole molecule) type. Among the first 10 transitions, pure π → π* (phenyl → phenyl) and n → π* type were not found for all six compounds.

Computational methods

All computations were performed on Gaussian 09[61] (AM64L-G09RevA.02, IBM64-G09RevA.02 and EM64L-G09RevA.02) and Gaussview 5.1 as GUI using default DFT functionals and basis sets. Optimizations were performed from structures built in

Table 5 Allowed (oscillator strength $f > 0$) electronic transitions (in order of increasing transition energy) of compounds **1**, **2**, **19**, **22**, **4** and **6** (singlets only) at SMD/TD-BMK/DGDZVP//SMD/B3LYP/DGDZVP level of theory in $CHCl_3$.All transitions to triplet excited states were found to be forbidden

Structure	*Transition*: orbitals	λ_{max} (nm)	*f* (a.u.)	TDM[a] (a.u.)
1	*1*: 82(HOMO) → 83(LUMO)	551	1.2139	22.0280
	4: 77,81 → 83	308	0.0331	0.3362
	6: 75 → 83,85; 76 → 88	281	0.0001	0.0013
	8: 78 → 83; 82 → 85	271	0.0794	0.7044
	9: 78 → 83; 81 → 84; 82 → 85	269	0.7227	6.4094
2	*1*: 82(HOMO) → 83(LUMO)	434	1.0036	14.3506
	2: 82 → 84	301	0.5263	5.2157
	5: 79 → 85; 80 → 83; 81 → 87; 82 → 86	275	0.0229	0.2074
	8: 78 → 83	242	0.1238	0.9881
	10: 78,80 → 83; 80 → 84; 79 → 85; 81 → 86; 82 → 87	232	0.0361	0.2765
19	*1*: 82(HOMO) → 83(LUMO)	459	1.5016	22.6691
	3: 79 → 84; 80 → 83,	308	0.0342	0.3470
	8: 78 → 83; 81 → 84; 82 → 85	245	0.6159	4.9746
	9: 74,78 → 83; 81 → 84	243	0.1729	1.3839
22	*1*: 82(HOMO) → 83(LUMO)	444	1.2170	17.8016
	2: 81 → 83	324	0.0145	0.1541
	3: 80 → 83,85; 82 → 87	296	0.0170	0.1657
	4: 79 → 83,84; 82 → 84	285	0.0350	0.3284
	6: 79 → 83; 82 → 84, 85	279	0.3568	3.2716
	7: 78 → 83, 81 → 84, 82 → 85	258	0.1114	0.9469
	8: 74,78 → 83, 81 → 84	249	0.0808	0.6627
4	*1*: 90(HOMO) → 91(LUMO)	582	0.7197	13.8019
	4: 82,83,85 → 91; 83 → 93; 85 → 86	306	0.0299	0.3008
	5: 82,83,85 → 91	290	0.7627	7.2804
	7: 87 → 91; 88 → 92; 90 → 95	284	0.0258	0.2410
	10: 89 → 92; 90 → 93	269	0.3264	2.8948
6	*1*: 90(HOMO) → 91(LUMO)	362	0.7848	9.3693
	2: 90 → 92	286	0.2797	2.6329
	7: 87 → 91; 87 → 92; 88 → 93; 86,90 → 91; 85,89 → 90	244	0.0042	0.0336
	8: 83,86 → 91; 83 → 92; 84 → 98; 90 → 96	238	0.0200	0.1565
	9: 89 → 93; 90 → 96	230	0.0478	0.3627

[a] TDM = transition dipole moment.

Gaussview either through pre-optimization at HF[52]/3-21G[56] or directly at B3LYP[27,42]/DGDZVP[20,21] first in gas phase followed by re-optimization in implicit solvent (IEFPCM[24] or SMD[23]) with cut-off values for Maximum Force = 0.001500, RMS Force = 0.001000, Maximum Displacement = 0.006000, RMS Displacement = 0.004000. Optimizations at B3LYP[27,42]/DGTZVP[20,21] level of theory were performed at Gaussian default cut-off values (Maximum Force = 0.00450, RMS Force = 0.00300, Maximum Displacement = 0.001800, RMS Displacement = 0.001200). All optimized structures were confirmed to reside in their respective PEHS minima by having only positive vibrational frequencies in gas phase, and implicit (IEFPCM or SMD) solvents.

Conclusions

An accurate and computationally efficient procedure (SMD (toluene)/TD-BMK/DGDZVP//SMD (toluene)B3LYP/DGDZVP for predicting the electronic transition of Pechmann dye family of compounds has been developed and then applied to virtual screening of novel heterocyclic and core-rearranged analogs. A large percentage of exact exchange mixed with a pure DFT exchange functional was found to be optimal (BMK functional contains 42% of exact exchange). For Pechmann dyes (*exo*-5,5-dilactones) and their rearranged (*endo*-6,6-dilactone) counterparts in toluene, the best absolute deviation of λ(max) prediction of $\leq$6 nm is achieved. Larger deviations are observed for more polar solvents and/or N-containing analogs. The colour shifts of *N*-alkyl Pechmann-dye-derived lactams are due to conformational twisting of the phenyl rings relative to the core chromophores and can be explained qualitatively by changes in the HOMO and LUMO energies. All of the first 10 allowed electronic transitions are of $\pi \rightarrow \pi^*$, singlet type. Among these, HOMO–LUMO transitions had the highest intensities and large transition dipole moments, implying a significant charge transfer upon excitation.

Acknowledgements

This work was funded by Institute of Materials Research and Engineering and Institute of High Performance Computing, Agency for Science, Technology and Research (A*STAR), Singapore. EABK thanks A*STAR Computer Resources Centre (A*CRC) for generous unlimited grants of computing time on Axle, Cirrus and Fuji Linux clusters.

Notes and references

1 (*a*) D. Sholl and J. A. Steckel, *Density Functional Theory: A Practical Introduction*, Wiley-VCH, 2009; (*b*) W. Koch and M. C. Holthausen, *A Chemist's Guide to Density Functional Theory*, Wiley-VCH, 2000.
2 P. Hohenberg and W. Kohn, *Phys. Rev.*, 1964, **136**, B864.
3 J. M. Tao, J. P. Perdew, V. N. Staroverov and G. E. Scuseria, *Phys. Rev. Lett.*, 2003, **91**, 146401.
4 S. F. Sousa, P. A. Fernandes and M. J. Ramos, *J. Phys. Chem. A*, 2007, **111**, 10439.
5 (*a*) H. Zollinger, *Colour Chemistry: Syntheses, Properties and Applications of Organic Dyes and Pigments*, Wiley-VCH, 2003; (*b*) K. Hunger, *Industrial Dyes: Chemistry, Properties, Applications*, Wiley-VCH, 2003, and refs. cited therein.
6 E. Runge and E. K. U. Gross, *Phys. Rev. Lett.*, 1984, **52**, 997.
7 M. E. Casida, *J. Mol. Struct. (THEOCHEM)*, 2009, **914**, 3.
8 (*a*) D. Jacquemin, B. Mennucci and C. Adamo, *Phys. Chem. Chem. Phys.*, 2011, **13**, 16987; (*b*) I. Vasiliev, M. L. d. Puerto, M. Jain, A. Lugo-Solis and J. R. Chelikowsky, *J. Mol. Struct. (THEOCHEM)*, 2009, **914**, 115; (*c*) D. Jacquemin, V. Wahtelet, E. A. Perpète and C. Adamo, *J. Chem. Theory Comput.*, 2009, **5**, 2410; (*d*) S. Grimme, in *Reviews in Computational Chemistry*, ed. K. B. Lipkovitz, R. Larter, T. R. Cundari and D. B. Boyd, Wiley-VCH, 2004, vol. 20, pp. 153–218.
9 (*a*) J. Fabian, *Dyes Pigm.*, 2010, **84**, 36; (*b*) D. Jacquemin, E. A. Perpète, I. Ciofini and C. Adamo, *Acc. Chem. Res.*, 2009, **42**, 326; (*c*) D. Jacquemin, E. A. Perpète, G. E. Scuseria, I. Ciofini and C. Adamo, *J. Chem. Theory Comput.*, 2008, **4**, 123.
10 (*a*) L. L. Yang, L. S. Guo, Q. Q. Chen, H. F. Sun, J. Liu, X. X. Zhang, X. Pan and S. Y. Dai, *J. Mol. Graphics Modell.*, 2011, **34**, 1; (*b*) M. P. Balanay, C. V. P. Dipaling, S. H. Lee, D. H. Kim and K. H. Lee, *Sol. Energy Mater. Sol. Cells*, 2007, **91**, 1775; (*c*) R. M. Ma, P. Guo, H. J. Cui, X. X. Zhang, M. K. Nazeerudin and M. Grätzel, *J. Phys. Chem. A*, 2009, **113**, 10119.
11 H. von Pechmann, *Ber. Dtsch. Chem. Ges.*, 1882, **15**, 881.
12 M. T. Bogert and J. J. Ritter, *J. Am. Chem. Soc.*, 1924, **46**, 2871.
13 K. Bowden, R. Etemadi and R. J. Ranson, *J. Chem. Soc., Perkin Trans. 2*, 1991, 743.
14 H. Irikawa and N. Adachi, *Heterocycles*, 2005, **65**, 1385.
15 H. Irikawa and N. Adachi, *Heterocycles*, 2000, **53**, 135.
16 H. Irikawa, N. Adachi and H. Muraoka, *Heterocycles*, 1998, **48**, 1415.
17 E. Klingsberg, *Chem. Rev.*, 1954, **54**, 59.
18 T. B. Norsten, E. A. B. Kantchev and M. B. Sullivan, *Org. Lett.*, 2010, **12**, 4816.
19 E. A. B. Kantchev, T. B. Norsten, M. L. Y. Tan, J. J. Y. Ng and M. B. Sullivan, *Chem.–Eur. J.*, 2012, **18**, 695.
20 N. Godbout, D. R. Salahub, J. Andzelm and E. Wimmer, *Can. J. Chem.*, 1992, **70**, 560.
21 C. Sosa, J. Andzelm, B. C. Elkin, E. Wimmer, K. D. Dobbs and D. A. Dixon, *J. Phys. Chem.*, 1992, **96**, 6630.
22 J. Silver, M. T. Afmet, K. Bowden, J. R. A. Reynolds, A. Bashall, M. McPartlin and J. Trottee, *J. Mater. Chem.*, 1994, **4**, 1201.
23 A. V. Marenich, C. J. Cramer and D. G. Truhlar, *J. Phys. Chem. B*, 2009, **113**, 6378.
24 (*a*) J. Tomasi, B. Mennucci and R. Cammi, *Chem. Rev.*, 2005, **105**, 2999; (*b*) V. Barone, M. Cossi and J. Tomasi, *J. Chem. Phys.*, 1997, **107**, 3210; (*c*) S. Miertus, E. Scrocco and J. Tomasi, *Chem. Phys.*, 1981, **55**, 117.
25 S. H. Vosko, L. Wilk and M. Nusair, *Can. J. Phys.*, 1980, **58**, 1200.
26 A. D. Becke, *Phys. Rev. A: At., Mol., Opt. Phys.*, 1988, **38**, 3098.
27 C. Lee, W. Yang and R. G. Parr, *Phys. Rev. B*, 1988, **37**, 785.
28 J. P. Perdew, *Phys. Rev. B*, 1986, **33**, 8822.
29 (*a*) J. P. Perdew, K. Burke and M. Ernzerhof, *Phys. Rev. Lett.*, 1996, **77**, 3685; (*b*) J. P. Perdew, K. Burke and M. Ernzerhof, *Phys. Rev. Lett.*, 1997, **78**, 1396.
30 J. P. Perdew, K. Burke and Y. Wang, *Phys. Rev. B: Condens. Matter*, 1996, **54**, 16533.
31 J. M. Tao, J. P. Perdew, V. N. Staroverov and G. E. Scuseria, *Phys. Rev. Lett.*, 2003, **91**, 146401.
32 J. Toulouse, A. Savin and C. Adamo, *J. Chem. Phys.*, 2002, **117**, 10465.
33 C. Adamo and V. Barone, *J. Chem. Phys.*, 1998, **108**, 664.
34 P. M. W. Gill, *Mol. Phys.*, 1996, **89**, 433.
35 A. D. Boese and N. C. Handy, *J. Chem. Phys.*, 2001, **114**, 5497.
36 S. Grimme, *J. Comput. Chem.*, 2006, **27**, 1787.
37 A. D. Becke, *J. Chem. Phys.*, 1996, **104**, 1040.
38 T. Van Voorhis and G. E. Scuseria, *J. Chem. Phys.*, 1998, **109**, 400.
39 A. D. Boese and N. C. Handy, *J. Chem. Phys.*, 2002, **116**, 9559.
40 Y. Zhao, N. E. Schultz and D. G. Truhlar, *J. Chem. Phys.*, 2006, **125**, 194101.
41 A. J. Cohen and N. C. Handy, *Mol. Phys.*, 2001, **99**, 607.
42 A. D. Becke, *J. Chem. Phys.*, 1993, **98**, 5648.
43 H. L. Schmider and A. D. Becke, *J. Chem. Phys.*, 1998, **108**, 9624.
44 Y. Zhao and D. Truhlar, *Theor. Chem. Acc.*, 2008, **120**, 215.
45 A. D. Boese and J. M. L. Martin, *J. Chem. Phys.*, 2004, **121**, 3405.
46 A. D. Becke, *J. Chem. Phys.*, 1993, **98**, 1372.
47 T. Yanai, D. P. Tew and N. C. Handy, *Chem. Phys. Lett.*, 2004, **393**, 51.
48 Y. Tawada, T. Tsuneda, S. Yanagisawa, T. Yanai and K. Hirao, *J. Chem. Phys.*, 2004, **120**, 8425.
49 H. Iikura, T. Tsuneda, T. Yanai and K. Hirao, *J. Chem. Phys.*, 2001, **115**, 3540.
50 J.-D. Chai and M. Head-Gordon, *J. Chem. Phys.*, 2008, **128**, 084106.
51 J.-D. Chai and M. Head-Gordon, *Phys. Chem. Chem. Phys.*, 2008, **10**, 6615.

52 S. P. Karna and M. Dupuis, *J. Comput. Chem.*, 1991, **12**, 487.
53 C. J. Cramer, *Essentials of Computational Chemistry*, Wiley VCH, 2002, pp. 153–189.
54 A. D. Boese, J. M. L. Martin and N. C. Handy, *J. Chem. Phys.*, 2003, **119**, 3005.
55 (*a*) A. Schaefer, C. Huber and R. Ahlrichs, *J. Chem. Phys.*, 1994, **100**, 5829; (*b*) A. Schaefer, H. Horn and R. Ahlrichs, *J. Chem. Phys.*, 1992, **97**, 2571.
56 W. J. Pietro, M. M. Francl, W. J. Hehre, D. J. Defrees, J. A. Pople and J. S. Binkley, *J. Am. Chem. Soc.*, 1982, **104**, 5039.
57 (*a*) M. M. Francl, W. J. Pietro, W. J. Hehre, J. S. Binkley, D. J. DeFrees, J. A. Pople and M. S. Gordon, *J. Chem. Phys.*, 1982, **77**, 3654; (*b*) W. J. Hehre, R. Ditchfield and J. A. Pople, *J. Chem. Phys.*, 1972, **56**, 2257; (*c*) R. Ditchfield, W. J. Hehre and J. A. Pople, *J. Chem. Phys.*, 1971, **54**, 724.
58 (*a*) A. D. McLean and G. S. Chandler, *J. Chem. Phys.*, 1980, **72**, 5639; (*b*) K. Raghavachari, J. S. Binkley, R. Seeger and J. A. Pople, *J. Chem. Phys.*, 1980, **72**, 650.
59 D. E. Woon and T. H. Dunning Jr., *J. Chem. Phys.*, 1993, **98**, 1358.
60 M. Hayashi, F. Toshimitsu, R. Sakamoto and H. Nishihara, *J. Am. Chem. Soc.*, 2011, **133**, 14518.
61 M. J. Frisch, G. W. Trucks, H. B. Schlegel, G. E. Scuseria, M. A. Robb, J. R. Cheeseman, G. Scalmani, V. Barone, B. Mennucci, G. A. Petersson, H. Nakatsuji, M. Caricato, X. Li, H. P. Hratchian, A. F. Izmaylov, J. Bloino, G. Zheng, J. L. Sonnenberg, M. Hada, M. Ehara, K. Toyota, R. Fukuda, J. Hasegawa, M. Ishida, T. Nakajima, Y. Honda, O. Kitao, H. Nakai, T. Vreven, J. Montgomery, J. A., J. E. Peralta, F. Ogliaro, M. Bearpark, J. J. Heyd, E. Brothers, K. N. Kudin, V. N. Staroverov, R. Kobayashi, J. Normand, K. Raghavachari, A. Rendell, J. C. Burant, S. S. Iyengar, J. Tomasi, M. Cossi, N. Rega, N. J. Millam, M. Klene, J. E. Knox, J. B. Cross, V. Bakken, C. Adamo, J. Jaramillo, R. Gomperts, R. E. Stratmann, O. Yazyev, A. J. Austin, R. Cammi, C. Pomelli, J. W. Ochterski, R. L. Martin, K. Morokuma, V. G. Zakrzewski, G. A. Voth, P. Salvador, J. J. Dannenberg, S. Dapprich, A. D. Daniels, Ö. Farkas, J. B. Foresman, J. V. Ortiz, J. Cioslowski and D. J. Fox, *Gaussian 09, Revision A.02*, Wallingford, CT, 2009.

